greatly appreciate that E. P. Bakker, R. A. Bogomolni, R. H. Lozier, and G. Wagner allowed us to read their manuscripts not yet in print.

References

Altendorf, K., Hirata, H., and Harold, F. M. (1975), *J. Biol. Chem. 250,* 1405.
Bakker, . P., Rottenberg, H., and Caplan, S. R. (1976), *Biochim. Biophys. Acta* (submitted).
Bogomolni, R. A., Baker, R. A., Lozier, R. H., and Stoeckenius, W. (1976), *Biochim. Biophys. Acta 440,* 68.
Chu Kung, M., DeVault, D., Hess, B., and Oesterhelt, D. (1975), *Biophys. J. 15,* 907.
Dencher, N., and Wilms, M. (1975), *Biophys. Struct. Mech. 1,* 259.
Harold, F. M. (1970), *Adv. Microbiol. Physiol. 4,* 45.
Harold, F. M., Baarda, J. R., and Pavlasova, E. (1970), *J. Bacteriol. 101,* 152.
Harold, F. M., and Papineau, D. (1972), *J. Membr. Biol. 8,* 45.
Hirata, H., Altendorf, K., and Harold, F. M. (1973), *Proc. Natl. Acad. Sci. U.S.A. 70,* 1804.
Hoeberichts, J. A., and Borst-Pauwels, G. W. F. H. (1975), *Biochim. Biophys. Acta 413,* 248.
Kanner, B. I., and Racker, E. (1975), *Biochem. Biophys. Res. Commun. 64,* 1054.
Lanyi, J. K., Renthal, R., and MacDonald, R. E. (1976a), *Biochemistry 15,* 1603.
Lanyi, J. K., Yearwood-Drayton, V., and MacDonald, R. E. (1976b), *Biochemistry 15,* 1595.
Lozier, R. H., Bogomolni, R. A., Niederberger, W., and Stoeckenius, W. (1976), *Biochim. Biophys. Acta* (submitted).
Lozier, R. H., Bogomolni, R. A., and Stoeckenius, W. (1975), *Biophys. J. 15,* 955.
MacDonald, R. E., and Lanyi, J. K. (1975), *Biochemistry 14,* 2882.
Mitchell, P. (1969), *Theor. Exp. Biophys. 2,* 160.
Mitchell, P. (1970), *Symp. Soc. Gen. Microbiol. 20,* 121.
Mitchell, P. (1972), *J. Bioenerg. 3,* 5.
Oesterhelt, D. (1975), *Ciba Found. Symp. 31,* 147.
Oesterhelt, D., and Hess, B. (1973), *Eur. J. Biochem. 37,* 316.
Oesterhelt, D., and Stoeckenius, W. (1973), *Proc. Natl. Acad. Sci. U.S.A. 70,* 2853.
Renthal, R., and Lanyi, J. K. (1976), *Biochemistry 15,* 2136.
Schuldiner, S., and Kaback, H. R. (1975), *Biochemistry 14,* 5451.
Stoeckenius, W., and Lozier, R. H. (1974), *J. Supramol. Struct. 2,* 769.
Wagner, G. (1976), *Aust. J. Plant Physiol.* (in press).
West, I. C., and Mitchell, P. (1974), *Biochem. J. 144,* 87.
Zarlengo, M. H., and Schultz, S. C. (1966), *Biochim. Biophys. Acta 126,* 308.

Hummel–Dreyer Gel Chromatographic Procedure as Applied to Ligand-Mediated Association†

John R. Cann* and Norman D. Hinman‡

ABSTRACT: A mass transport theory of the gel chromatographic procedure of Hummel and Dreyer for measuring the binding of small ligand molecules to macromolecules has been formulated for ligand-mediated macromolecular association. It is concluded that the Hummel–Dreyer procedure is the method of choice for quantitating ligand binding in such systems. Guidelines are drawn for unambiguous interpretation of the nonclassical elution profiles in terms of the number of binding sites on the macromonomer and their intrinsic binding constant. Most of these guidelines also apply to static equilibrium methods such as equilibrium dialysis.

Hummel and Dreyer (1962) introduced the following gel chromatographic procedure for quantitating the binding of a small ligand molecule, X, by a protein or other macromolecule, M. After equilibration of a column of Sephadex (G-25 or other grade which excludes M) with X, M dissolved in the solution used to equilibrate the column is applied. The column is then eluted with the same solution as used for equilibration, and the effluent is analyzed for X. As the band of M moves down the column in the exterior mobile phase, it removes X from the solution within the gel until the binding equilibrium is satisfied by the concentration of unbound X ahead of M. Subsequently, M and its complexes with X emerge from the column at its void volume to give a peak in the elution profile of X, followed at some point by a trough. The amount of X removed from solution by the protein as manifested by the trough is equal to the excess X in the peak. The mean number of mol of X bound/mol of M, ν, can be calculated using the area of the trough or the void volume peak depending, in practice, upon how the effluent is monitored for X: if by ultraviolet spectrophotometry (Fairclough and Fruton, 1966) the area of the trough must be used, since the protein contributes to the absorbance of the void volume fractions; if by determination of radioactivity (Levi et al., 1974), the area of the peak can be

† From the Department of Biophysics and Genetics, University of Colorado Medical Center, Denver, Colorado 80220. *Received March 29, 1976.* Publication no. 655. Supported in part by Research Grant 5R01 HL13909-24 from the National Heart and Lung Institute, National Institutes of Health, United States Public Health Service.

‡ Present address: Biochemistry Department, Eastern Virginia Medical School, Norfolk, Va. 23507.

used. Each experiment of this kind gives ν at an equilibrium concentration of X equal to the concentration of X in the solution used for initial equilibration of the column. These data are then analyzed in the same way as those from equilibrium dialysis (Klotz and Hunston, 1971; Steinhardt and Beychok, 1964; Scatchard, 1949) to give the number of binding sites on the protein molecule and their binding constant(s).

The described behavior is for ideal systems uncomplicated by changes in the state of aggregation of the protein induced by ligand binding. One might expect rather different elution profiles unamenable to classical interpretation for systems undergoing reversible ligand-mediated association, because, conceivably, association would enhance or might even inhibit ligand binding, depending upon reaction mechanism and ratio of ligand to macromolecule concentration. Such experiments are beginning to appear in the literature (Levi et al., 1974; Lee et al., 1975; Wilson et al., 1975). Accordingly, theoretical profiles have been calculated for a variety of model systems in order to ascertain how the equilibrium constant and the stoichiometry of the binding reaction per se can best be determined experimentally. The results of these calculations are, in turn, compared with those for equilibrium dialysis and other static methods not involving mass transport, which show even severer departure from classical behavior when applied to ligand-mediated association.

In order to insure against unwarranted generalizations concerning the analysis of ligand-binding data on associating systems, it was necessary to examine in some detail a rather large number of model systems. Of these, the following were chosen to illustrate the principles involved: The completely cooperative interaction (reaction 1)

$$mM + mX \rightleftharpoons M_mX_m,\ m = 2, 4, \text{and } 6 \qquad (1)$$

the sequential monomer–tetramer reaction (reaction set II)

$$\begin{gathered} M + X \rightleftharpoons MX,\ K_1 \\ 4MX \rightleftharpoons M_4X_4,\ K_2 \end{gathered} \qquad (2)$$

the sequential and progressive tetramerization

$$\begin{gathered} M + X \rightleftharpoons MX,\ K_1 \\ 2MX \rightleftharpoons M_2X_2,\ K_2 \\ MX + M_2X_2 \rightleftharpoons M_3X_3,\ K_3 \\ MX + M_3X_3 \rightleftharpoons M_4X_4,\ K_4 \\ K_2 = K_3 = K_4 \equiv K_a \end{gathered} \qquad (3)$$

the monomer–dimer reaction

$$\begin{gathered} M + X \rightleftharpoons MX,\ K_1 \\ M + MX \rightleftharpoons M_2X,\ K_2 \end{gathered} \qquad (4)$$

the monomer–dimer–trimer reaction

$$\begin{gathered} M + X \rightleftharpoons MX,\ K_1 \\ M + MX \rightleftharpoons M_2X,\ K_2 \\ MX + M_2X \rightleftharpoons M_3X_2,\ K_3 \\ K_2 = K_3 \equiv K_a \end{gathered} \qquad (5)$$

and the elaborated monomer–dimer–trimer reaction

$$\begin{gathered} M + X \rightleftharpoons MX,\ K_1 \qquad M + M_2X_2 \rightleftharpoons M_3X_2,\ K_6 \\ M + MX \rightleftharpoons M_2X,\ K_2 \qquad MX + M_2X_2 \rightleftharpoons M_3X_3,\ K_7 \\ 2MX \rightleftharpoons M_2X_2,\ K_3 \qquad M_2X + X \rightleftharpoons M_2X_2,\ K_8 \\ M + M_2X \rightleftharpoons M_3X,\ K_4 \qquad M_3X + X \rightleftharpoons M_3X_2,\ K_9 \\ MX + M_2X \rightleftharpoons M_3X_2,\ K_5 \qquad M_3X_2 + X \rightleftharpoons M_3X_3,\ K_{10} \\ K_2 = K_3 = K_4 = K_5 = K_6 = K_7 \equiv K_a \\ K_1 = K_8 = K_9 = K_{10} \equiv K \end{gathered} \qquad (6)$$

Reaction 1 says nothing about the mechanism of interaction other than its cooperativity. Reactions sets 2–5 schematize the ligand-mediated mechanism of reversible polymerization in which obligatory binding of ligand to the monomer must precede macromolecular association, and dissociation of the polymer(s) must precede release of ligand bound into the complex(es). Reaction set 6 is not purely mediated but contains an aspect of ligand-facilitated polymerization (Tai and Kegeles, 1975) in that the binding reactions governed by K_8, K_9, and K_{10} tend to stabilize the dimer and trimer formed via ligand mediation.

Theory

Static Equilibrium Methods. Equilibrium dialysis and comparable methods for measurement of ligand binding, which do not involve mass transport, were simulated by numerical solution of the mass action expressions for given constituent concentration of macromolecule, $\overline{C}_m$, and ligand, $\overline{C}_l$

$$\overline{C}_m = [M] + K_1[M][X] + 2K_1K_2[M]^2[X] \qquad (1a)$$

$$\overline{C}_l = [X] + K_1[M][X] + K_1K_2[M]^2[X] \qquad (1b)$$

whose simultaneous solution by the Newton–Raphson method (p 319 in Carnahan et al., 1969) gives the equilibrium concentrations, [ ], of M and X which, in turn, are used to calculate the quantities

$$[MX] = K_1[M][X] \qquad (2)$$

$$[M_2X] = K_1K_2[M]^2[X] \qquad (3)$$

$$\nu = ([MX] + [M_2X])/\overline{C}_m \qquad (4)$$

The results are displayed either as double-reciprocal plots (Klotz and Hunston, 1971) of $1/\nu$ vs. $1/[X]$ or as Scatchard plots (Scatchard, 1949) of $\nu/[X]$ vs. ν. It can be shown analytically that the intercept of the Scatchard plot with the ordinate for individual model systems is: reaction set 2, K_1; 3, K_1; 4, $K_1 + K_1K_2\overline{C}_m$; 5, $K_1 + K_1K_a\overline{C}_m$; and 6, $K + KK_a\overline{C}_m + KK_a^2\overline{C}_m^2$.

It can also be deduced analytically that for reaction set 4 the binding isotherm and, thus, both the double-reciprocal and Scatchard plots are stationary at their midpoint ($\nu = 0.5$), where $1/[X] = K_1$ independent of K_2 and $\overline{C}_m$.

Hummel–Dreyer Procedure. The theory to be described is for elution chromatography using a bed of gel which completely excludes the macromolecular species but is freely accessible to the unbound ligand. The computations are for the limiting case of reactions so fast relative to flow rate that, in effect, there is local equilibrium among the interacting species. Theoretical profiles of macromolecule and ligand concentration in the mobile phase vs. position along the chromatographic column were computed by numerical solution of the appropriate system of equations comprised of the continuity and mass-action equations for constituent macromolecule and constituent ligand. There is a close analogy between the equation of continuity for exchange of solute between stationary and mobile phase with simultaneous axial dispersion in gel chromatography, and the transport equations which conserve mass during sedimentation and electrophoresis. Likewise, the calculation can be described in analogous terms. Imagine that the chromatographic column is divided along its longitudinal axis into a number of discrete segments of length, Δx. Given the initial equilibrium concentrations of the several species in the mobile phase of each segment, we calculate the change in the longitudinal distribution of material during a short interval of time, Δt, due to chromatographic transport.

It is assumed that there is no reequilibration by interaction during Δt, each species being chromatographed independently from its distribution at the beginning of the interval. After the concentrations have been advanced, equilibrium is recalculated. That is, for known constituent concentrations of macromolecule and ligand computed from the concentrations of the several species as changed by chromatographic transport, new equilibrium concentrations are calculated by applying the law of mass action. We then compute the change in this new distribution of material due to transport over the next Δt, recalculate the equilibrium, and so on, thereby constructing the evolution of the longitudinal distribution of material in the mobile phase of the column from the initial condition.

The continuity equation for independent gel chromatography (Ackers, 1970) of the ith species in the reacting system is[1]

$$\frac{\partial C_i}{\partial t} = L_i \frac{\partial^2 C_i}{\partial x^2} - v_i \frac{\partial C_i}{\partial x} \tag{5}$$

where C_i is the molar concentration in the mobile phase, t is the time, and x is the longitudinal position in the chromatographic column. L_i is the axial dispersion coefficient and $v_i = F/\xi_i$ is the velocity imparted by the flow of eluate at a rate F. $\xi_i = \alpha + \beta\sigma_i$ is the distribution volume/unit length, σ_i is the partition coefficient, α is the void volume/unit length, and β is the internal volume/unit length. All of the macromolecular species have the same partition coefficient, $\sigma_m = 0$, while for unbound ligand, $\sigma_l = 1$. Equation 5 has been solved in a frame of reference moving with the velocity of the macromolecular species, $v_m = F/\alpha$, which introduces the new position variable $x' = x - v_m t$. When transformed into the moving coordinate system eq 5 becomes

$$\frac{\partial C_k}{\partial t} = L_k \frac{\partial^2 C_k}{\partial x'^2} \tag{6a}$$

for the kth macromolecular species, and

$$\frac{\partial C_l}{\partial t} = L_l \frac{\partial^2 C_l}{\partial x'^2} - (v_l - v_m) \frac{\partial C_l}{\partial x'} \tag{6b}$$

for unbound ligand.

We now introduce discrete time and position variables: $t_n = n\Delta t$, $n = 0, 1, 2, \ldots$; $x'_j = j\Delta x'$, $j = 0, 1, 2, \ldots J$; and replace the continuous variables $C_k(t, x')$ and $C_l(t, x')$ by the discrete variables $C_k(n\Delta t, j\Delta x') \equiv C_k(t_n, x'_j)$ and $C_l(n\Delta t, j\Delta x') \equiv C_l(t_n, x'_j)$. In most cases, eq 6a,b was approximated by explicit finite difference equations as described previously (see eq 2a in Cann, 1973), but for the more complicated models (e.g., reaction sets 3 and 4), the implicit Crank–Nicholson method (p 451 in Carnahan et al., 1969) was used to difference the differential equations. In the Crank–Nicholson method the first and second spatial derivatives are taken to vary linearly with time between their values at the beginning and end of each time interval, Δt. Not only is this a more accurate representation but, more important, the difference equations are unconditionally stable provided that the first spatial derivative is differenced in the forward direction (Cann, 1973). This affords a significant saving of computer time, since larger values of Δt may be used in the calculation. It should be noted, however, that the calculation is still subject to the truncation error due to the way the first spatial derivative is approximated (Goad and Cann, 1969). Application of the Crank–Nicholson method to eq 6b, for example, yields the difference equation (subscript l on C dropped for simplicity)

$$\frac{C(t_{n+1}, x'_j) - C(t_n, x'_j)}{\Delta t} = \frac{L_l}{2(\Delta x')^2} \times \{[C(t_{n+1}, x'_{j-1}) - 2C(t_{n+1}, x'_j) + C(t_{n+1}, x'_{j+1})] + [C(t_n, x'_{j-1}) - 2C(t_n, x'_j) + C(t_n, x'_{j+1})]\} - \frac{(v_l - v_m)}{2\Delta x'} \{[C(t_{n+1}, x'_{j+1}) - C(t_{n+1}, x'_j)] + [C(t_n, x'_{j+1}) - C(t_n, x'_j)]\} \tag{7}$$

Given values of C at any time t, we can calculate their values at $t + \Delta t$ as changed by chromatography using this equation. But, since it involves values of $C(t_{n+1}, x'_{j'})$ at segments j' that flank j, the equation at each j contains as unknowns the concentrations at three segments, and the following system of linear equations involving $J - 1$ unknowns and two boundary values must be solved

$$-\lambda C(t_{n+1}, x'_{j-1}) + [1 + 2\lambda - G]C(t_{n+1}, x'_j) - [\lambda - G]C(t_{n+1}, x'_{j+1}) = \lambda C(t_n, x'_{j-1}) + [1 - 2\lambda + G]C(t_n, x'_j) + (\lambda - G)C(t_n, x'_{j+1}),$$

$$\lambda = \frac{L_l \Delta t}{2(\Delta x')^2}, \quad G = \frac{(v_l - v_m)\Delta t}{2\Delta x'}, \quad j = 1, 2, \ldots J - 1 \tag{8}$$

Solution is accomplished by Gaussian elimination as described in detail on pp 441–442 in Carnahan et al. (1969).

At each time, t_{n+1}, new values of $\bar{C}_m$ and $\bar{C}_l$ are computed from C_k and C_l as changed by transport, and reequilibration is imposed essentially as described above under *Static Equilibrium Methods*. The new values of the equilibrium concentrations serve as the starting distribution of material for the next time cycle of chromatography followed by reequilibration, and so on. Given initial conditions and boundary values, this recursive calculation allows one to follow the evolution of the Hummel–Dreyer profile.

The initial conditions depend upon the initial location in the space grid of the mixture of macromolecule and ligand applied to the column equilibrated with ligand at concentration $[X]_c$. In many calculations the initial zone was centered in the space grid such that

$$C_k(0, x'_j) = [k\text{th macromolecular species}]^\circ,$$
$$C_l(0, x'_j) = [X]^\circ, \bar{C}_l = [X]_c, j = J/2 - 5, \ldots J/2 + 5$$
$$C_k(0, x'_j) = 0, \quad C_l(0, x'_j) = [X]_c, \quad j = J/2 - 5, \ldots J/2 + 5$$

where $[\ ]^\circ$ denoted initial equilibrium concentration. The boundary values are

$$C_k(t_n, 0) = C_k(t_n, x'_J) = 0, C_l(t_n, 0) = C_l(t_n, x'_J) = [X]_c$$

Computations were made on the University of Colorado's CDC 6400 electronic computer using $\Delta x' = 0.03 - 0.1$ cm and $\Delta t = 5$–20 s, except for a control calculation to be discussed below in which $\Delta t = 30$ s. Column parameters were $\alpha = 0.295$, $\beta = 0.670$, $L_p = 3.62 \times 10^{-2}$ cm^{-1}, and $qd^2 = 5.4 \times 10^{-6}$ cm^2, corresponding to Sephadex G-75 (Halverson and Ackers, 1971; Zimmerman et al., 1971). Values of L were calculated from eq 6 in Zimmerman et al. (1971) using the following values for the diffusion coefficients: ligand, 10^{-5} cm^2 s^{-1}; macromonomer, $D_1 = 4 \times 10^{-7}$ cm^2 s^{-1}; and m-mer, $D_m = D_1/m^{1/3}$.

[1] The continuity equation as formulated here only appears to make the assumption of instantaneous equilibration of solute between the exterior mobile phase and the solution within the beads of gel. Actually, the nonequilibrium perturbation resulting from the finite rate of diffusional distribution between the two phases is embodied in the axial dispersion coefficient (Ackers, 1970).

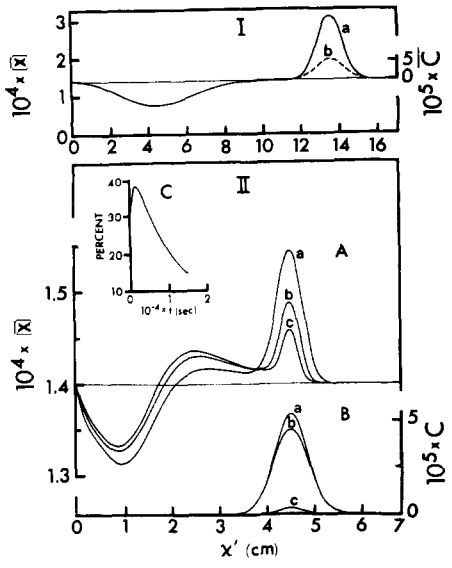

FIGURE 1: Theoretical Hummel-Dreyer profiles. (I) Control calculation for the reaction, $M + 4X \rightleftharpoons MX_4$; $K = 1.04 \times 10^{16}$ M^{-4}; $\bar{C} = 8.75 \times 10^{-5}$ M initially; $[X]_c = 1.4 \times 10^{-4}$ M; $t = 4.5 \times 10^4$ s: curve a, Hummel-Dreyer profile; curve b, macromolecule profile of $\bar{C}$ vs. x'. The value $\nu = 3.18$, as calculated from composition of peak, is to be compared with the equilibrium value, $\nu = 3.20$, for $[X] = [X]_c$. (II) Calculated for reaction 1 with 30% m-merization at initial $\bar{C} = 1.4 \times 10^{-4}$ M and $[X]_c = 1.4 \times 10^{-4}$ M: (A) Hummel-Dreyer profiles for $n = 2$ (curve a), $n = 4$ (curve b), and $n = 6$ (curve c) at $t = 1.5 \times 10^4$ s. (B) Profile of macromolecule corresponding to curve b in A: a, $\bar{C}$; b, [M]; and c, $[M_4X_4]$. (C) Plot of percent tetramerization at apex of macromolecule profile against time during evolution of curve b in A. $F = 0.36$ ml h^{-1}, $v_m = 3.384 \times 10^{-4}$ cm s^{-1}, and $v_l - v_m = -2.353 \times 10^{-4}$ cm s^{-1} throughout. The fact that the width of the initial band of macromolecule in I is three times the width in II accounts for the fortuitous agreement between the heights of the macromolecule profiles.

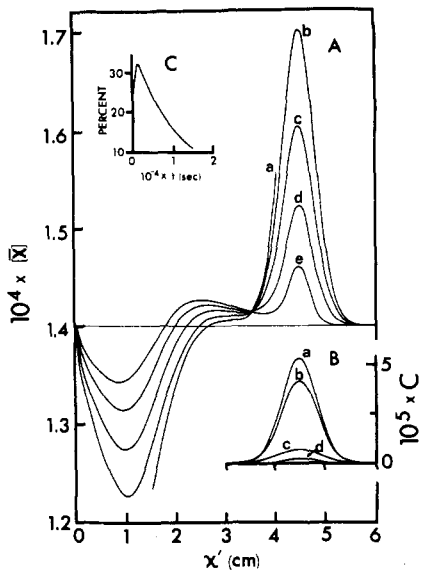

FIGURE 2: Theoretical Hummel-Dreyer profiles calculated for reaction set 2 with 25% tetramerization initially. (A) Hummel-Dreyer profiles: curve a, $K_1 = 1.91 \times 10^4$ M^{-1} and $K_2 = 1.15 \times 10^{12}$ M^{-3}; curve b, 7.14×10^3 and 5.83×10^{12}; curve c, 2.92×10^3 and $4\,50 \times 10^{13}$; curve d, 1.05×10^3 and 1.05×10^{15}; and curve e, 9.62×10^1 and 7.49×10^{18}. All other parameters as in Figure 1-II. (B) Macromolecule profile corresponding to curve d in A: a, $\bar{C}$; b, [M]; c, [MX]; and d, $[M_4X_4]$. (C) Plot of percent tetramer at apex of macromolecule profile against time during evolution of curve d in A.

(Note that the third term on the right hand side of this equation is dropped in the case of the macromolecular species, because they are completely excluded from the beads of gel.)

The following simplified notation was adopted for displaying the results of the calculations: C is generic for molar concentration of macromolecule; $\bar{C}$ denotes the constituent concentration of macromolecule; as defined previously, [X] is the equilibrium molar concentration of ligand; $[\bar{X}]$ denotes the constituent concentration of ligand; as before, $[X]_c$ is the concentration of ligand used to equilibrate the chromatographic column. Theoretical Hummel-Dreyer profiles are displayed as plots of $[\bar{X}]$ vs. x'; profiles of macromolecule, $\bar{C}$ or C vs. x'. The distance that the peak of macromolecule moves down the column is $d = v_m t$, which corresponds to the volume of eluate, $V = Ft$. Chromatographic transport was of sufficient duration that the concentration of unbound ligand within the peak of macromolecule approached $[X]_c$ to within 0.001-0.1% in the vast majority of cases and within 1-2% in most others.

Since the coordinate system moves with the velocity of the macromolecule, the truncation error due to the way in which the first spatial derivative is approximated applies only to the ligand and acts to increase its axial dispersion by an amount $|v_l - v_m|\Delta x'/2$ (Goad and Cann, 1969). The influence of this "truncation dispersion" on the shape of the Hummel-Dryer profile was minimized as described previously (Cann and Kegeles, 1974), in some cases completely compensating for the error. With the more complex reaction sets 3 and 6, a compromise with respect to the size of $\Delta x'$ was dictated by practical considerations of the computer time required for calculation; the larger $\Delta x'$, the larger is "truncation dispersion". In these cases, only about one-third of the error could be compensated for, but this is tolerable, since pilot calculations showed that the major influence of "truncation dispersion" is to increase the spreading of the trough in the profile with negligible effect (<0.002%) on the amount of ligand bound to the macromolecule.

Finally, a brief consideration of errors other than "truncation dispersion" are in order. In the control calculation displayed in Figure 1-I the area of the trough is about 8% greater than the area of the peak, although (1) the overall ligand material balance is good to about 1%, (2) the protein material balance is good to better than 0.002%, and (3) the value of ν calculated from the composition of the peak agrees to 0.6% with the equilibrium value for $[X] = [X]_c$. The discrepancy between the areas is attributed to the truncation error due to the way in which the time derivative is approximated, which is $O(\Delta t)$ for the explicit difference equations (Richtmeyer and Morton, 1967). When the value of Δt was reduced from 30 to 10 s, the discrepancy decreased to about 5% with material balance good to about 0.5%. A different kind of error is shown by the profiles displayed in Figures 1-IIA and 2A, the area of the trough being about 10% smaller than the area of the two peaks with overall ligand material balance good to about 0.1%. Here, the discrepancy is due to the fact that the concentration of unbound ligand was significantly perturbed in segment $j = 1$ next to the segment in which the boundary value $C_l(t_n, 0) = [X]_c$ was imposed. Under this circumstance, segment $j = 0$ in effect acts as a source from which ligand diffuses into the trough. When Δt is sufficiently small and care is taken not to disturb the concentration of ligand in the segments adjacent to $j = 0$, the area of the trough agrees with the area of the peak(s) to within 0.003% (Figure 4) with excellent material balance to about 3×10^{-6}%. These conditions obtain in the calculations for reaction sets 3-6 inclusive.

Assessment of Theoretical Profiles. The following expla-

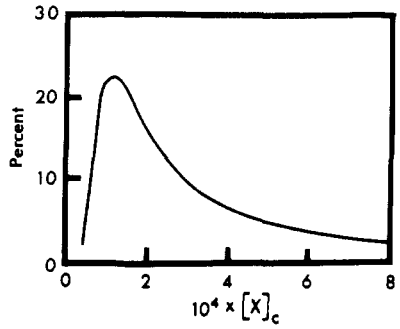

FIGURE 3: Plot of the relative area of the peak of released ligand; percent of total area of the peaks of released and bound ligand vs. the concentration of ligand used to equilibrate the Hummel-Dryer column, $[X]_c$, for reaction set 2 with values of macromolecule concentration and other parameters corresponding to curve d in Figure 2A.

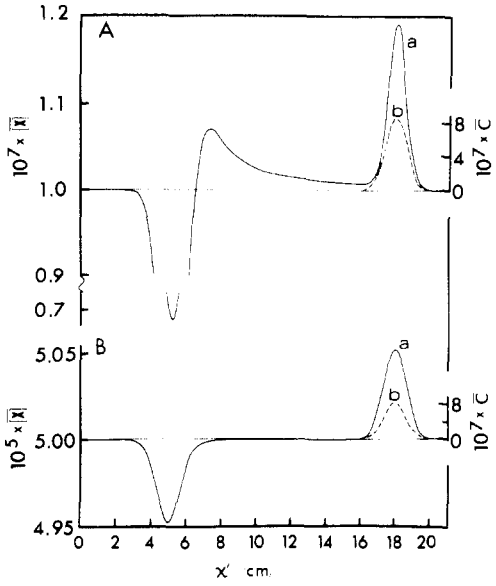

FIGURE 4: Effect of the concentration of ligand used to equilibrate the chromatographic column upon the shape of the theoretical Hummel-Dreyer profile (curve a), calculated for reaction set 4 with $K_1 = 5 \times 10^4$ M^{-1} and $K_2 = 4.5 \times 10^6$ M^{-1}. (A) $[X]_c = 1 \times 10^{-7}$ M and $\nu = 0.0175$ as calculated from the composition of the peak of bound ligand; (B) $[X]_c = 5 \times 10^{-5}$ M and $\nu = 0.633$. Curve b is the macromolecule profile, $\bar{C}$ vs. x'. Initially $\bar{C} = 4.55 \times 10^{-6}$ M, $F = 2$ ml h^{-1}, $v_m = 1.885 \times 10^{-3}$ cm s^{-1}, $v_l - v_m = -1.309 \times 10^{-3}$ cm s^{-1}, and $t = 9.98 \times 10^3$ s.

nation of the moving-coordinate system and the concentration frame of reference used in the calculations serves to place the theoretical Hummel-Dreyer profiles into proper experimental perspective. First, let us refer to Figure 1-I for clarification of the moving-coordinate system, $x' = x - v_m t$. When the zone of macromolecule admixed with ligand was applied to the equilibrated column at $t = 0$, it was centered at $x' = x = 13.50$ cm. During simulated chromatography, the peak of macromolecule remained at this location as the coordinate system moved to the left with the velocity of the macromolecular species, $v_m = 3.389 \times 10^{-4}$ cm s^{-1}. By the time $t = 4.497 \times 10^4$ s of chromatography, the starting position had moved from $x' = x = 13.50$ cm to $x' = 13.50 - 3.389 \times 10^{-4} \times 4.497 \times 10^4 = -1.74$ cm. In other words, the macromolecule moved the distance d = 13.50 + 1.74 = 15.24 cm down the column. Simultaneously, the trough in the ligand profile formed and moved, d = 4.23 + 1.74 = 5.97 cm. Perhaps, this can be seen more clearly by transforming back to the stationary coordinate system in which the macromolecule was initially centered at $x = 13.50$ cm. After chromatography, the macromolecule was centered at $x = x' + v_m t = 28.74$ cm, and the trough at $x = 19.47$ cm. One may make other linear transformations such as assigning $x = 0$ to the initial position, in which case $x = 5.97$ cm for the trough and 15.24 cm for the macromolecule.

The concentrations represented in the profiles displayed in Figures 1, 2, and 4 correspond to those in the mobile phase within the column rather than to those in the effluent. Thus, the theoretical profiles do not have exactly the same shapes as would be obtained experimentally in elution volume profiles. In particular, the peaks and trough in the elution profile would be broader than in the computed one, but this has little, if any, consequences for the conclusions reached in this study, since integration of the areas in the elution profile would provide the same information. Nor are the theoretical profiles quite the same as would be obtained by direct optical scanning of the column (Ackers, 1970) which measures solute concentrations with respect to the total column, mobile plus stationary phase; here too the same information is embodied in the experimental profiles and is readily retrievable.

Results

The results of the calculations are presented below in a format which first considers theoretical predictions as to the shape of Hummel-Dreyer profiles for ligand-mediated association and then turns to the problem of quantitative interpretation of the profiles in terms of stoichiometry and binding constants. Ample comparisons are drawn between the Hummel-Dreyer procedure and static methods, such as equilibrium dialysis, in order to emphasize that the same precautions and guidelines for interpretation of raw binding data apply to both.

Shape of Hummel-Dreyer Profiles. The control calculation displayed in Figure 1-I shows that in the absence of ligand-mediated macromolecular association the shape of the theoretical Hummel-Dreyer profile is classical, even for cooperative binding of ligand. In contrast, the shape of the profile can depart markedly from classical expectation for ligand-mediated association, as illustrated in Figures 1-IIA and 2A for reaction 1 and reaction set 2, respectively. Typically, the profile shows a peak of ligand associated with the peak of macromolecule (Figures I-IIB and 2B) followed by a peak of unbound ligand, which, in turn, is followed by a trough. This behavior is understood as follows. As the initially narrow band of macromolecule departs from the top of the chromatographic column to begin its passage down the column in the exterior mobile phase, it removes ligand from the solution within the gel until the simultaneous ligand-binding and macromolecular association equilibria are satisfied with respect to the concentration of ligand ahead. This is the process which gives rise to the trough. At the same time, however, the concentration of macromolecule and its complexes decreases continuously as the band spreads due to axial dispersion. Consequently, macromolecular association is reversed by mass action with concomitant release of ligand bound into the m-mers. The released ligand lags behind the advancing band of macromolecule and would form a long, trailing plateau in the profile if macromolecular dissociation could proceed unabated. Actually, however, the amount of m-mer decreases progressively during passage down the column. In addition, the rate of spreading of the band, $d(\overline{x'^2} - \overline{x'}^2)^{1/2}/dt$, decreases virtually[2] as $t^{-1/2}$, so that dilution and, thus, dissociation of the re-

[2] "Virtually", because the average axial dispersion coefficient of the macromolecule increases slightly with time as m-mer dissociates.

maining m-mer also decrease. Consequently, the concentration of released ligand must pass through a maximum to form a peak which skews forward to blend into the peak of bound ligand. These several processes are illustrated graphically in Figures 1-IIC and 2C, which show that the relative amount of m-mer passes through a maximum, at first increasing as ligand is withdrawn from the gel and then decreasing as a result of dissociation within the spreading band.

The area of the peak of released ligand as compared to the peak of bound ligand is governed by several factors, foremost of which is the order of macromolecular association. The higher the order of association, other things held constant, the larger is the relative area of the peak of released ligand (Figure 1-IIA). This is a direct consequence of the law of mass action; the concentration of higher-order m-mers being more sensitive to the dilution, which occurs in the spreading band. For a given order of association, the relative area of the peak increases with increasing ratio of the macromolecular association constant to the binding constant (Figure 2A), because the extent of enhancement of ligand binding by the association reaction increases with the strength of association. Finally, the relative area is sensitive to the concentration of ligand used to equilibrate the chromatographic column, the exact functional relationship depending upon reaction mechanism. For the sequential monomer-tetramer reaction set 2, the relative area passes through a maximum with increasing ligand concentration (Figure 3). The area at first increases because there is an increasing amount of tetramer to dissociate in the spreading band with concomitant release of ligand. At higher $[X]_c$, however, another mass-action effect dominates; namely, the overall reaction is driven so strongly to the right (i.e., $K_1^4K_2[X]_c^4 = [M_4X_4]/[M]^4$ increases so markedly) that there is progressively less dissociation of tetramer upon dilution. For certain other models (e.g., reaction set 4) the profile (Figure 4) shows a peak of released ligand only at low $[X]_c$ where dimerization enhances ligand binding. At higher $[X]_c$, dimerization inhibits binding by removing unliganded monomer from the reaction arena. Consequently, dissociation of the dimer in the spreading zone does not release ligand, rather it favors further ligand binding.

Interpretation of Hummel-Dreyer Profiles. We now address ourselves to the problem of quantitative interpretation of the nonclassical Hummel-Dreyer profiles shown by ligand mediated associating systems. The questions posed are the following. "Should the composite of the peaks of released and bound ligand (corresponding in practice to the area of the trough) or the peak of bound ligand be used to calculate ν"? "Should one employ a double-reciprocal plot or a Scatchard plot to determine the number of binding sites and the apparent binding constant"? "How can the actual binding constant be derived"? "Do not similar considerations also apply to the interpretation of data from static equilibrium experiments"? Unambiguous answers required examination of several different model systems.

Let us first consider reaction set 2, which is a cooperative interaction in the sense that tetramerization of the liganded monomer enhances ligand binding at all ligand concentrations. As a consequence of the cooperativity, the double-reciprocal plots of theoretical binding data (curves a, b, and c in Figure 5A) are concave toward the abscissa and extrapolate to the ordinate with a very flat slope. Whereas the intercept with the ordinate and, thus through reciprocity, the number of binding sites on the monomer are readily determined, the apparent binding constant (K_{app}), given by the quotient of the intercept and the limiting slope, is not the intrinsic binding constant (K_1)

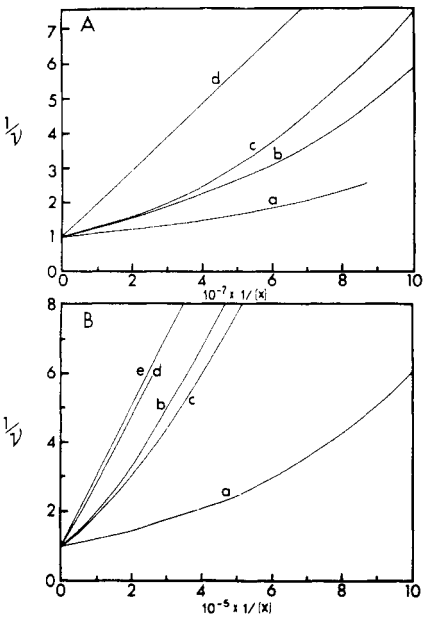

FIGURE 5: Theoretical double-reciprocal plots of ligand-binding data. (A) Calculated for reaction set 2 with $K_1 = 1.05 \times 10^3\ M^{-1}$ and $K_2 = 1.05 \times 10^{15}\ M^{-3}$: a, static equilibrium methods, $\bar{C} = 1.4 \times 10^{-4}$ M; b, Hummel-Dreyer procedure using composite of the peaks of released and bound ligand to calculate ν; c, Hummel-Dreyer method using peak of bound ligand to calculate ν; d, limit of infinite dilution of macromolecule, where $\nu = K_1[X]/(1 + K_1[X])$. For the Hummel-Dreyer calculations, $\bar{C} = 1.4 \times 10^{-4}$ M initially, $[X] = [X]_c$; $v_m = 3.39 \times 10^{-4}$ cm s^{-1}, and $t = 1.5 \times 10^4$ s. (B) Calculated for reaction set 3 with $K_1 = 5 \times 10^4\ M^{-1}$ and $K_a = 1 \times 10^5\ M^{-1}$; a, static equilibrium, $\bar{C} = 1.4 \times 10^{-4}$ M; b, static equilibrium, $\bar{C} = 1.4 \times 10^{-5}$ M; c, Hummel-Dreyer with $\bar{C} = 1.4 \times 10^{-4}$ M initially, $v_m = 1.88 \times 10^{-3}$ cm^2 s^{-1}, and $t = 1 \times 10^4$ s; d, Hummel-Dreyer, $\bar{C} = 1.4 \times 10^{-4}$ M initially; and e, limit of infinite dilution.

but rather some weighted average of K_1 and the tetramerization constant (K_2). Moreover, this departure from the classical prediction for nonassociating systems (curve d) is even more severe for static equilibrium measurements (curve a) than for Hummel-Dreyer experiments (curves b and c), because the dilution of macromolecule inherent to the chromatographic procedure decreases the role of tetramerization. In principle, extrapolation to infinite dilution of K_{app} values determined at progressively lower macromolecule concentration should eliminate the role of tetramerization completely to give K_1, but, as shown in Figure 6, the extrapolation would be uncertain in practice because of the sigmoid shape of the plot. In passing, we note that Figure 6 also illustrates the corollary that the larger K_2, the greater is the departure from classical behavior. Since the use of double-reciprocal plots in the present context clearly leaves something to be desired, we make appeal to Scatchard plots.

The Scatchard plots of the theoretical binding data displayed in Figure 7A reflect the cooperativity of the reaction by their open downward shape. While they extrapolate to the abscissa in a straightforward manner to give the correct number of binding sites on the monomer, their approach to the intercept with the ordinate is marred by a small toe. This means that, in practice, linear extrapolation to the ordinate would underestimate the value of K_1: by about 25% for static equilibrium measurements, about 20% for Hummel-Dreyer data obtained from the composite of the peaks of released and bound ligand (i.e., the trough in the profile), and only about 8% for Hummel-Dreyer data from the peak of bound ligand. Thus, both chemical intuition and theory tell us that, whenever possible, the area of the peak of bound ligand should be used to calculate

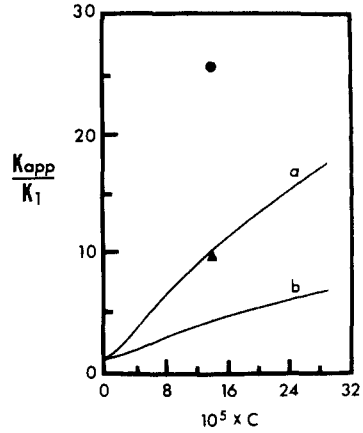

FIGURE 6: Plot of the ratio (K_{app}/K_1) of apparent binding constant given by double-reciprocal plots to the intrinsic binding constant vs. the concentration of macromolecule (C) showing extrapolation to infinite dilution; calculated for reaction set 2 with $K_1 = 1.05 \times 10^3$ M^{-1} and $K_2 = 1.05 \times 10^{15}$ M^{-3} for the two curves, and $K_1 = 1.05 \times 10^3$ M^{-1} and $K_2 = 4.29 \times 10^{16}$ M^{-3} for the two points: curve a and point ●, static equilibrium methods for which $C \equiv \bar{C}$; curve b and point ▲, Hummel-Dreyer procedure for which $C \equiv \bar{C}$ initially.

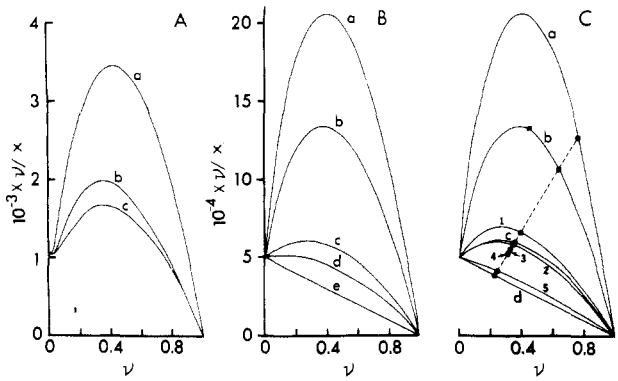

FIGURE 7: Theoretical Scatchard plots of ligand-binding data. (A) Calculated for reaction set 2; curves a, b, and c same as in Figure 5A. (B) Calculated for reaction set 3; static equilibrium methods with $K_1 = 5 \times 10^4$ M^{-1} and $\bar{C} = 1.4 \times 10^{-4}$ M: a, $K_a = 1 \times 10^5$ M^{-1}; b, 5×10^4 M^{-1}; c, 1×10^4 M^{-1}; d, 5×10^{-3} M^{-1}; and e, limit for either $K_a = 0$ or infinite dilution of macromolecule. (C) Calculated for reaction set 3 with $K_1 = 5 \times 10^4$ M^{-1} and $K_2 = 1 \times 10^5$ M^{-1}; curves a, b, and c are for static equilibrium with $\bar{C} = 1.4 \times 10^{-4}$, 7×10^{-5}, and 1.4×10^{-5} M, respectively, curve d, limit of infinite dilution. Curves 1 and 2, points 3 and 4, and curve 5 are for the Hummel-Dreyer procedure with $F = 2$ ml h^{-1}, $v_m = 1.88 \times 10^{-3}$ cm s^{-1}, and the following values for other parameters: $\bar{C} = 1.4 \times 10^{-4}$ M initially, except for curve 5 where $\bar{C} = 1.4 \times 10^{-5}$ M; $t = 1 \times 10^4$, 2×10^4, 3×10^4, 4×10^4, and 1×10^4 s, respectively; d = 18.8, 37.7, 56.5, 75.4, and 18.8 cm, respectively. Isochore (- - -) connects points of equal equilibrium concentration of ligand, 6×10^{-6} M.

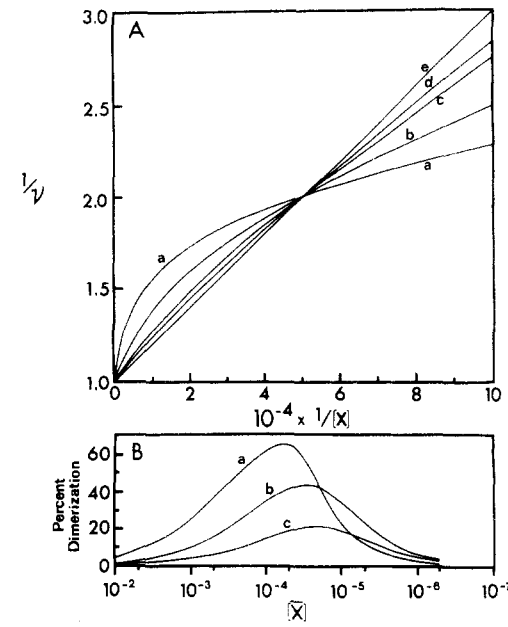

FIGURE 8: Theoretical ligand-binding data for reaction set 4 with $K_1 = 5 \times 10^4$ M^{-1} and $K_2 = 1.5 \times 10^5$ M^{-1}. (A) Double-reciprocal plots: a, b, and c are for static equilibrium methods with $\bar{C} = 7.27 \times 10^{-5}$, 1.8×10^{-5}, and 4.55×10^{-6} M, respectively; d, Hummel-Dreyer procedure, $\bar{C} = 1.8 \times 10^{-5}$ M initially and other parameters as given in legend to Figure 4; e, limit of infinite dilution of macromolecule. (B) Plots of percent dimerization at static equilibrium against constituent concentration of ligand; a, b, and c relate to curves a, b, and c in Figure A, respectively.

ν, and we adopted this guideline in all of the theoretical calculations that follow.

The properties and Hummel-Dreyer behavior of interactions which are cooperative in macromolecules were explored further in calculations on the sequential and progressive tetramerization reaction set 3. For this model system, the Scatchard plots, which are also open downward in shape (Figures 7B,C), extrapolate smoothly to the ordinate to give K_1. The contrast between the simplicity of this treatment of the data and the corresponding double-reciprocal plots presented in Figure 5B is telling.

The calculations for static equilibrium methods displayed in Figure 7B show how very sensitive ligand binding can be to the macromolecular association which it mediates, while the comparisons drawn in Figure 7C define conditions which are applicable to the quantification of ligand-mediated association reactions in general. Thus, we see the advantage conferred upon the Hummel-Dreyer procedure by the dilution of macromolecule, which results from axial dispersion (compare curve 1 with curve a), and the longer the chromatographic column, the closer the system converges upon the limit in which association no longer enhances ligand binding (Follow the isochore from curve 1 to point 4.) It is also apparent that, in practice, the limit can be approached more efficiently by applying a lower concentration of macromolecule to a column of moderate length (compare curve 5 with curve 1), provided that the sacrifice of some analytical precision can be tolerated.

Granted these generalizations which emerge in a natural way from consideration of cooperative interactions, it remains so that other reaction mechanisms will give double-reciprocal and Scatchard plots whose shapes and interpretation differ markedly from those shown by cooperative interactions. This is well illustrated by calculations for the monomer–dimer reaction set 4. The double-reciprocal plots displayed in Figure 8A have a shape reminiscent of nonassociating systems characterized by heterogeneity of binding sites with respect to their intrinsic affinity for ligand. In the case of the associating system, the shape reflects the fact that, whereas the dimerization reaction enhances ligand binding at concentrations of ligand less than the midpoint concentration, dimerization actually inhibits binding at higher ligand concentrations by removing unliganded monomer from the reaction arena. Moreover, when the strength of ligand binding is the same order of magnitude or weaker than dimerization, very high concentrations of ligand are required to reverse the dimerization reaction (Figure 8B) via binding to the released unliganded monomer, thereby driving the binding reaction to completion. This explains the steep descent of curve a in Figure 8A to its intercept with the ordinate. Obviously, it is difficult, if not impossible, to extract intrinsic binding constants from such plots. Fortunately, the

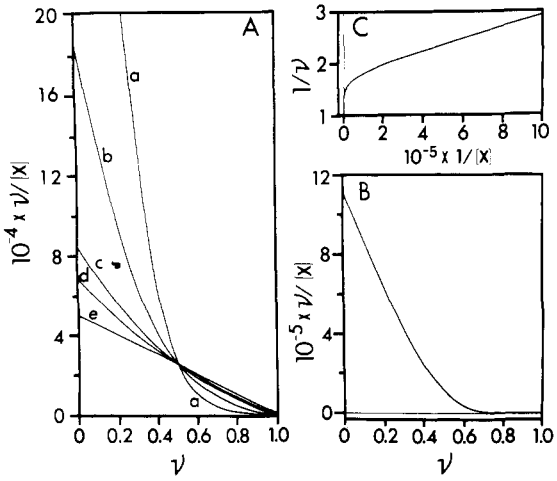

FIGURE 9: Theoretical ligand-binding data: (A) Scatchard plots of the same data displayed in Figure 8A as double-reciprocal plots. (B) Scatchard plot for reaction set 5 with either $K_1 = 5 \times 10^4$ M^{-1}, $K_a = 1.5 \times 10^5$ M^{-1}, and $\bar{C} = 1.4 \times 10^{-4}$ M, or $K_1 = 5 \times 10^4$ M^{-1}, $K_a = 1.5 \times 10^6$ M^{-1}, and $\bar{C} = 1.4 \times 10^{-5}$ M; static equilibrium methods. (C) Double-reciprocal plot of same binding data as in B.

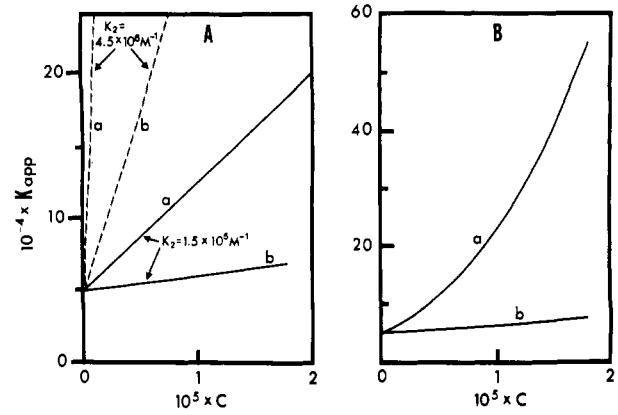

FIGURE 10: Extrapolation of apparent binding constant, K_{app}, from Scatchard plot to infinite dilution of macromolecule. (A) Calculated for reaction set 4 with $K_1 = 5 \times 10^4$ M^{-1}: a, static equilibrium methods, $C \equiv \bar{C}$ (to within 1% the slope equals K_1K_2 as predicted analytically); b, Hummel-Dreyer procedure, $C \equiv \bar{C}$ initially and other parameters as given in legend to Figure 4. (B) Calculated for reaction set 6 with $K = 5 \times 10^4$ M^{-1} and $K_a = 1.5 \times 10^5$ M^{-1}: a, static equilibrium (agrees with the analytically predicted quadratic curve to within 0.6%); b, Hummel-Dreyer with same column parameters as for b in A.

corresponding Scatchard plots (Figure 9A) are transparent, although still reminiscent of heterogeneous systems in being concave toward the abscissa. The apparent binding constant, as given by the quotient of the intercept with the ordinate and the number of binding sites from the intercept with the abscissa, is readily extrapolated to infinite dilution of macromolecule to yield the intrinsic binding constant.[3] In agreement with analytical prediction for this model system, the extrapolation is linear (Figure 10A). This is so for the Hummel-dreyer procedure, as well as static equilibrium methods, because of our assumption of rapid equilibration relative to flow rate and the constancy of time of chromatography and column parameters. It is important to note, however, that the linearity is not a generalization; the extrapolation being predictably curvilinear for reaction set 4 (Figure 10B).

Finally, a word of caution concerning determination of the number of binding sites on the monomer is in order. Thus, extrapolation of the Scatchard plot to the abscissa can be subject to considerable error, as illustrated by curve a in Figure 9A and the plot displayed in Figure 9B for the monomer-dimer-trimer reaction set 5. The latter plot approaches very close to the abscissa at $\nu \sim 0.7$ and then hugs the abscissa as it slowly converges to the actual number of binding sites at $\nu = 1$. Nor can the number of sites be determined from a double-reciprocal plot of the binding data, since, as shown in Figure 9C, the curve now approaches the ordinate at $1/\nu \sim 1.5$ and then hugs the ordinate as it converges to $1/\nu = 1$. This behavior is a direct consequence of mass action, as illustrated in Figure 11: namely, dimerization and trimerization are sufficiently strong that it requires extremely high concentrations of ligand to drive the dissociation of m-mers via binding to the concomitantly released unliganded monomer. If experimentally it is impractical to make measurements at sufficiently low macromolecule concentration so as to lift the Scatchard plot from the abscissa (e.g., curves c and d in Figure 9A), the intercepts on the ordinate can still be used to determine the binding constant to the first site.

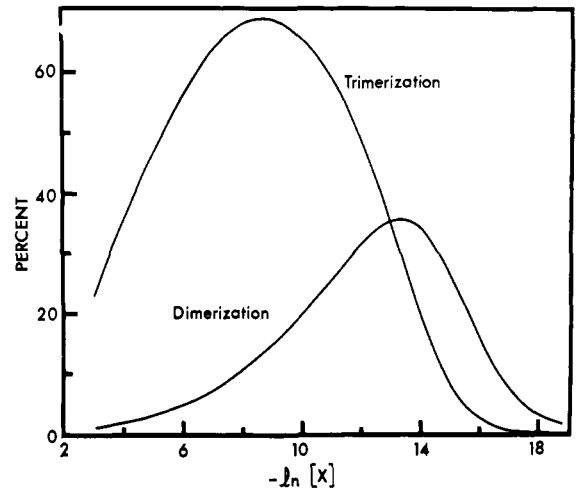

FIGURE 11: Plots of percent dimerization and percent trimerization against equilibrium concentration of ligand; in exact correspondence with the calculation displayed in Figures 9B,C.

Discussion

The conclusion reached in this study is that the gel chromatographic procedure of Hemmel-Dreyer (1962) is the method of choice for quantitating ligand binding when the ligand mediates association of the macromolecule. In fact, the theoretically predicted shape of the elution profile for ligand-mediated association may prove to be diagnostic for such interactions. Profiles showing a peak of bound ligand followed by a peak or broad shoulder of unbound ligand and, subsequently, a trough have been observed experimentally with two associating systems: the binding of GTP by tubulin in microtubule-reassembly buffer (Levi et al., 1974) and the binding of vinblastine by tubulin (Lee et al., 1975; Wilson et al., 1975). Our calculations provide the following guidelines for unambiguous interpretation of Hummel-Dreyer profiles when it is known or suspected that the ligand induces association of the protein. (1) Whenever possible, the area of the peak of bound

[3] All of the results reported here are for model systems which assume a single binding site on the monomer, but unpublished equilibrium calculations for a model system with two binding sites having the same intrinsic affinity for ligand generalize this conclusion. If the binding sites happen to be heterogeneous, the extrapolation to infinite dilution gives the arithmetic mean intrinsic binding constant (Klotz and Hunston, 1971).

ligand, rather than the area of the trough, should be used to calculate the mol of ligand bound/mol of macromolecule. (2) Double-reciprocal plots of the binding data must be avoided. (3) The intrinsic binding constant is determined by extrapolating the apparent binding constant given by the Scatchard plots to infinite dilution of macromolecule. (If the Scatchard plot is open downward in shape, extrapolation to infinite dilution may be superfluous.) (4) The extrapolation need not be linear. All but the first also apply to static equilibrium methods.

Although these guidelines were arrived at by computer simulation using model systems, a model is not required for interpretation of experimental binding data. This is so because the extrapolation to infinite dilution erases the role of association in determining the extent of ligand binding at finite macromolecule concentrations. Having determined the number of binding sites on the macromonomer and their intrinsic binding constant, the mechanism of the ligand-mediated association can be elucidated through application of independent biophysical methods, such as ultracentrifugation, light scattering, and rapid kinetic measurements (Lee et al., 1975; Frigon and Timasheff, 1975; Morimoto and Kegeles, 1971; Tai and Kegeles, 1975).

It is instructive to show how the theoretical calculations apply explicitly to binding studies on the GTP–tubulin and vinblastine–tubulin systems. In the case of the GTP–tubulin system (Levi et al., 1974), the number of moles of GTP bound/mole of tubulin was measured in reassembly buffer as a function of GTP concentration using the Hummel–Dreyer procedure. Values of ν were determined from the composition of the void-volume peak of bound ligand rather than from the trough in the elution profiles, but the data were analyzed by means of double-reciprocal plots. The plots are very flat and yield a binding constant which, in view of the theoretical results displayed in Figures 5 and 6, is probably artifactually large. The theory indicates that the experiments should be repeated at several different concentrations of tubulin, preferably in a buffer which does not support reassembly. Apparent binding constants should be determined from Scatchard plots and extrapolated to infinite dilution of tubulin in order to obtain the intrinsic binding constant.

Turning to the interaction of vinblastine with tubulin, the theoretical calculations indicate that interpretation of binding experiments on this system must take cognizance of the fact that the drug induces association of the protein (Lee et al., 1975). Lee et al. (1975) present a Scatchard plot of Hummel–Dreyer data for binding of vinblastine to calf brain tubulin. The data are fitted to a straight line (their Figure 4), although it would appear to us that the data may actually describe a curve concave toward the abscissa, as in Figure 9A. It is possible that linearization of the data accounts for the apparent stoichiometry of $n = 1.8$, rather than an integer. A more serious concern is the order of magnitude difference between their value, $2.2 \times 10^4\ M^{-1}$, for the binding constant and the value, $8.2 \times 10^5\ M^{-1}$, obtained by Wilson et al. (1975) for embryonic chick brain tubulin using a Scatchard plot of binding data determined by a static equilibrium method. These investigators also fitted to a straight line data which would seem to describe a curve concave to the abscissa (read individual sets of measurements in their Figure 2). Although the difference in binding constant values obtained in these two studies might be species related, it could instead be a consequence of different degrees of vinblastine-induced association under the different experimental conditions. In any case, it is to be expected that this apparent discrepancy will resolve itself once binding measurements, which define as precisely as possible the shape of the Scatchard plots, are made at different tubulin concentrations, and the apparent binding constants are extrapolated to infinite dilution to obtain the intrinsic constant.

Lastly, the results of our calculations have conceptual implications for qualitative interpretation of graphical representations of binding data. Thus, a concave downward (negative curvature) double-reciprocal plot (e.g., Figure 8A) or a concave upward (positive curvature) Scatchard plot (e.g., Figures 9A,B) need not necessarily be indicative of heterogeneity of binding sites with respect to their intrinsic affinity for ligand. Ligand-mediated associating systems with homogeneous sites can also give such plots.

References

Ackers, G. K. (1970), *Adv. Protein Chem. 24,* 343.

Cann, J. R. (1973), *Biophys. Chem. 1,* 1.

Cann, J. R., and Kegeles, G. (1974), *Biochemistry 13,* 1868.

Carnahan, B., Luther, H. A., and Wilkes, J. O. (1969), Applied Numerical Methods, New York, N.Y., Wiley.

Fairclough, G. F., Jr., and Fruton, J. S. (1966), *Biochemistry 5,* 673.

Frigon, R. P., and Timasheff, S. N. (1975), *Biochemistry 14,* 4559, 4567.

Goad, W. B., and Cann, J. R. (1969), *Ann. N.Y. Acad. Sci. 164,* 172.

Halvorson, H. R., and Ackers, G. K. (1971), *J. Polym. Sci., Polym. Phys. Ed. 9,* 245.

Hummel, J. P., and Dreyer, W. J. (1962), *Biochim. Biophys. Acta 63,* 530.

Klotz, I. M., and Hunston, D. L. (1971), *Biochemistry 10,* 3065.

Lee, J. C., Harrison, D., and Timasheff, S. N. (1975), *J. Biol. Chem. 250,* 9276.

Levi, A., Cimino, M., Mercanti, D., and Calissano, P. (1974), *Biochim. Biophys. Acta 365,* 450.

Morimoto, K., and Kegeles, G. (1971), *Arch. Biochem. Biophys. 142,* 247.

Richtmyer, R. D., and Morton, K. W. (1967), Difference Methods for Initial-Value Problems, 2nd Ed., New York, N.Y., Interscience, p. 189.

Scatchard, G. (1949), *Ann. N.Y. Acad. Sci. 51,* 660.

Steinhardt, J., and Beychok, S. (1964), *Proteins 2nd Ed.,* Vol. II, New York, N.Y., Academic Press, Chapter 8.

Tai, M.-S., and Kegeles, G. (1975), *Biophys. Chem. 3,* 307.

Wilson, L., Creswell, K. M., and Chin, D. (1975), *Biochemistry 14,* 5586.

Zimmerman, J. K., Cox, D. J., and Ackers, G. K. (1971), *J. Biol. Chem. 246,* 4242.